Printed with permission of The Institute of Pure and Applied Physics (IPAP)

JAPANESE JOURNAL OF APPLIED PHYSICS Vol.42 (2003) pp.1-15
Part1 No.1, January 2003
Invited Review Paper

Base-Metal Electrode-Multilayer Ceramic Capacitors: Past, Present and Future Perspectives

Hiroshi KISHI, Youichi MIZUNO and Hirokazu CHAZONO

Multilayer ceramic capacitor (MLCC) production and sales figures are the highest among fine-ceramic products developed in the past 30 years. The total worldwide production and sales reached 550 billion pieces and 6 billion dollars, respectively in 2000. In the course of progress, the development of base-metal electrode (BME) technology played an important role in expanding the application area. In this review, the recent progress in MLCCs with BME nickel (Ni) electrodes is reviewed from the viewpoint of nonreducible dielectric materials. Using intermediate-ionic-size rare-earth ion (Dy_2O_3, Ho_2O_3, Er_2O_3, Y_2O_3) doped $BaTiO_3$ (ABO_3)-based dielectrics, highly reliable Ni-MLCCs with a very thin layer below 2μm in thickness have been developed. The effect of site occupancy of rare-earth ions in $BaTiO_3$ on the electrical properties and microstructure of nonreducible dielectrics is studied systematically. It appears that intermediate-ionic-size rare-earth ions occupy both *A*- and *B*-sites in the $BaTiO_3$ lattice and effectively control the donor/acceptor dopant ratio and microstructural evolution. The relationship between the electrical properties and the microstructure of Ni-MLCCs is also presented.

KEYWORDS: multilayer ceramic capacitors, base metal electrode, nickel, barium titanate, dopants, rare-earth elements, site occupancy, reliability, dielectric properties, microstructure

1. Introduction

Recently, in mobile electronic equipment such as cellular phones and personal computers, trends toward miniaturization, higher performance, and lower electric power consumption have become increasingly prominent. Integration and miniaturization into chips of passive components such as capacitors, inductors, and resistors used in these pieces of equipment have also been accelerated. Conventionally, single-layer ceramic capacitors such as disk and cylindrical-type capacitors have been primarily used. However, the use of multilayer ceramic capacitors (MLCCs) prevails nowadays, because of their properties of high capacitance with small size, high reliability, and excellent high-frequency characteristics.[1] Figure 1 shows a change in the global shipment of MLCCs in the past ten years, compared with shipments of cellular phones and computers.[2] The quantity of shipment of MLCCs has grown at an annual rate of about 15% due to the rapid increase of the production of cellular phones and computers, and the demand will further increase in the future. The case size of MLCC also has been reduced every year. The current mainstream Electrical Industry Alliance (EIA)

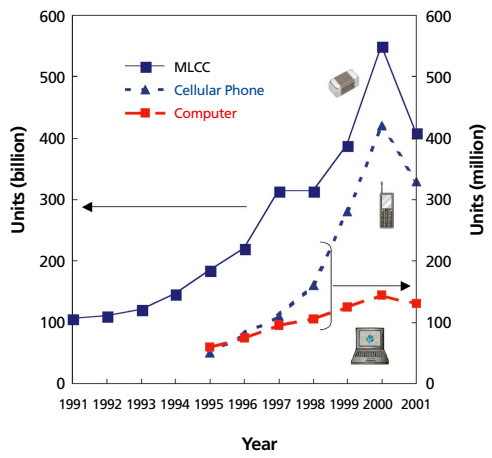

Fig. 1. Change in production volume of MLCCs in the world (after EIA WCTS data[2]).

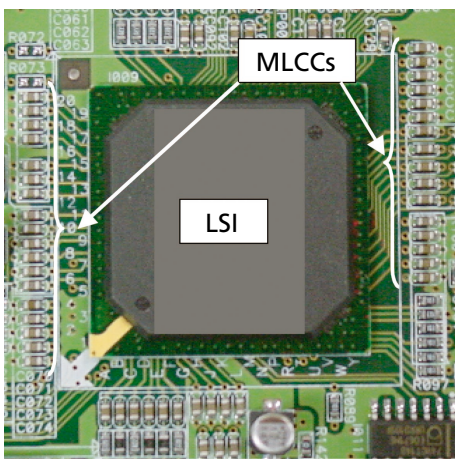

Fig. 2. Example of MLCC application in LSI circuit.

General R&D Laboratories, Taiyo Yuden Co., Ltd., 5607-2 Nakamuroda, Haruna-machi, Gunma-gun, Gunma 370-3347, Japan
(Received November 1, 2002; accepted for publication November 6, 2002)

case size is 0603 (1.6 by 0.8 mm^2) for general electronic equipment and EIA0402 (1.0 by 0.5 mm^2) for mobile equipment. The MLCC with EIA0201 (0.6 by 0.3 mm^2) case size is also being put into practical use. Furthermore, as shown in Fig. 2, the use of large-capacitance MLCCs of 1 to 100μF is rapidly expanding in several circuits for LSI, replacing tantalum capacitors and aluminum electrolytic capacitors which have been primarily used. The MLCC, as shown in Fig. 3, has a structure in which many dielectric layers and internal electrodes are alternately stacked and the internal electrodes are connected in parallel. The capacitance C of the MLCC is represented by

$$C = \varepsilon_r \cdot \varepsilon_0 \cdot (n-1) \cdot s/t, \quad (1)$$

where s is the overlap area of internal electrodes, n is the number of the internal electrode layers, ε_r is the relative dielectric constant (K) of the dielectric ceramic, t is the thickness of the dielectric layer, and ε_0 is the dielectric constant of free space.

Thus, requirements for achieving large-capacitance MLCCs with small size include using higher K value of a dielectrics, thinning of dielectric layers, increasing number of stacked layers, increasing overlap area of internal electrodes, and improving stacking precision. MLCCs were fabricated by the following method. Sheeting and printing methods are used in practice for forming the dielectric layers. An electrode paste of fine internal electrode powder is applied by screen-printing onto a dielectric green sheet. A predetermined number of printed sheets are stacked, pressed, and cut into pieces. After burning out the binder, the chips are fired. In order to sinter both the ceramic and electrode, it is important to control sintering shrinkage behavior of each material and the firing conditions.

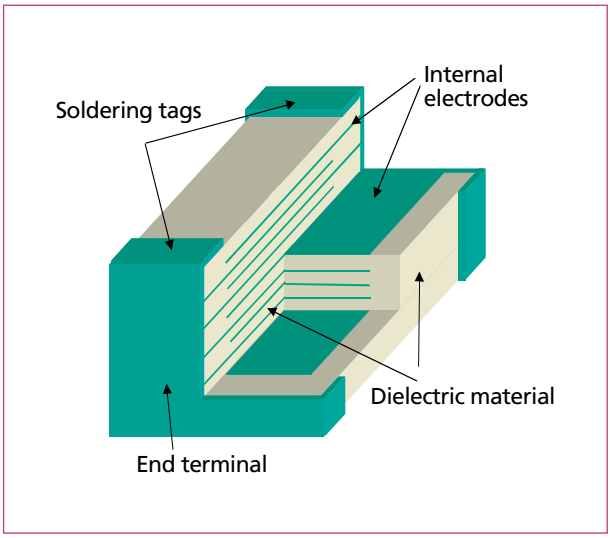

Fig. 3. Cut-away view of multilayer ceramic capacitor.

Conventional MLCCs based on $BaTiO_3$ (ABO_3) have been fabricated with noble metals such as platinum (Pt) or palladium (Pd) as internal electrodes which can be fired with dielectrics in air at 1300°C or higher. With an increased number of stacked layers due to miniaturization and higher capacitance of MLCCs, the proportion of the electrode cost to the overall cost increases steeply. Thus, a cost reduction of the internal electrodes has been intensively investigated for reducing the cost of MLCCs.

Methods for reducing the internal electrode cost are classified into 1) use of silver (Ag)–Pd alloy electrodes having a high Ag content (more than 70%) to achieve low-temperature sintering of the dielectrics and 2) use of base metals such as nickel (Ni) and copper (Cu) as internal electrodes by using a nonreducible dielectric that can be fired in a reducing atmosphere. Table I shows the physical properties and price ratio of various electrode materials for MLCCs. Table II sum-

Table I. Physical properties and price ratio of various electrodes.

Metals	Melting point(°C)	Resistivity(mΩ)	Firing atmosphere	Price ratio
Ag	961	1.62	Air	3
Cu	1080	1.72	Reducing	1
Ni	1453	6.9	Reducing	1
Pd	1552	10.4	Air	80

Table II. Typical ceramic dielectric materials for MLCCs with several EIA specifications.

EIA designation	Class	Temp. range (°C)	Temp.–cap. change (%)	K value up to	BT content (%)	Other dopants	Grain size (μm)
NPO(C0G)	1	–55 to 125	±30 ppm	100	10–50	TiO_2, $CaTiO_3$, $Nd_2Ti_2O_7$	1
X7R(BX)	2	–55 to 125	±15	4,000	90–98	MgO, MnO, Nb_2O_5, CoO Rear-earth	<1.5
Z5U	2	10 to 85	+22, –56	14,000	80–90	$CaZrO_3$, $BaZrO_3$	3–10
Y5V	2	–30 to 85	+22, –82	18,000	80–90	$CaZrO_3$, $BaZrO_3$	3–10

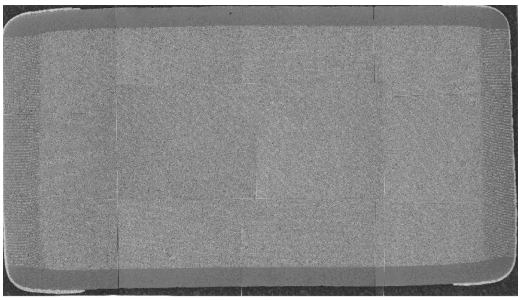

Fig. 4. Cross sectional view of EIA 1812 case size (4.5 by 3.2 mm²) X7R 100μF Ni-MLCC. Dielectric layer thickness = 1.8 μm, number of layers = 700.

marizes several ceramic dielectric materials for MLCCs in the EIA specifications.

For low-temperature-fired $BaTiO_3$-based dielectrics, addition of a low-melting-point glass component and addition of LiF have been investigated.[3–8] The problem in these materials is their low *K* value due to the addition of the low-melting-point additives which have low *K*. Around the end of the 1980s, Burn *et al*.[9] developed high *K* value Y5V and X7R dielectrics which can be fired below 1100°C by the addition of a $BaO–ZnO–B_2O_3–SiO_2$ glass component and are compatible with a 70% Ag–30% Pd electrode. The typical *K* values for Y5V and X7R materials were 15000 and 3000, respectively.

Other dielectrics that can be sintered at low temperatures below 1100°C, i.e., Pb-based complex perovskite materials having higher dielectric constants than $BaTiO_3$, have been intensively studied since the 1980s. The Pb-based complex perovskite dielectrics are ferroelectric materials discovered by Smolenskii *et al*.[10] in the 1950s and have a perovskite structure like $BaTiO_3$. The materials are represented by a general formula $Pb(B',B'')O_3$ where Pb occupies the *A*-site and multiple cations having different valences occupy the *B*-site. Since Yonezawa *et al*.[11] developed a $Pb(Fe_{1/3}W_{2/3})O_3–Pb(Fe_{1/2}Nb_{1/2})O_3$ -based material for MLCCs for practical applications, $Pb(Mg_{1/2}W_{1/2})O_3$, $Pb(Mg_{1/3}Nb_{2/3})O_3$ and $Pb(Zn_{1/3}Nb_{2/3})O_3$-based dielectrics have been intensively investigated for practical applications.[12–16] These dielectric materials, which can be sintered below 1000°C, enable the use of Ag–Pd alloy electrodes having high silver contents, and exhibit excellent electrical characteristics, for example, a *K* value for the Y5V characteristic of 25000 or more with satisfactory dc bias characteristics.

As another method for reducing electrode costs, replacement of the Pd electrode with base metal electrodes composed of Ni or Cu has been intensively investigated for practical applications in the 1980s. Ni and Cu are easily oxidized in air at high temperatures. Hence, the dielectric materials must be fired in a reducing atmosphere. However, conventional dielectrics are readily reduced under such a firing condition and become semiconductive as represented by

$$BaTiO_3 + xH_2 \rightarrow BaTiO_{3-X} + xH_2O \quad (2)$$

$$O_O \rightarrow 1/2O_2(g) + V_O^{\bullet\bullet} + 2e'. \quad (3)$$

Therefore, for BME applications, it is important to develop nonreducible dielectrics that can maintain high insulation resistance after firing in a reducing atmosphere. In the case of use of Cu electrodes, low-temperature sintering below the melting point of Cu (MP=1080°C) is required in addition to nonreducibility.

In the second half of the 1990s, a sudden rise in Pd prices has accelerated non-use of Pd as internal electrodes, and concern about environmental contamination by lead (Pb) compounds in electronic components has rapidly promoted the use of base metals such as Ni and Cu in low-cost MLCC development. With progress in fabrication technology of thin sheets and development of nonreducible dielectrics capable of using inexpensive Ni in internal electrodes, the production of Ni-MLCCs has markedly increased with a focus on large-capacitance products. During the past decade, the thickness of the dielectric layer has reduced from 10μm to about 2 μm, and MLCCs composed of 500 or more laminated layers have already been mass-produced. Figure 4 shows the cross-sectional view of an EIA 1812 case size (4.5 by 3.2 mm²) X7R 100μF Ni-MLCC. At present, 50% or more of MLCC products with high capacitance use Ni electrodes, and the share of the Ni-MLCCs will further increase in the future. In this paper, we will describe the development of nonreducible dielectrics suitable for thin-dielectric-layer Ni-MLCCs with large capacitance and also present the electrical properties and reliability of Ni-MLCCs. Some of the future perspectives of BME MLCCs are also discussed.

2. Development of Nonreducible Dielectrics for Ni-MLCCs

The study on $BaTiO_3$-based nonreducible dielectrics for producing Ni-MLCCs was initiated by Herbert[17] in the early 1960s. Up to the 1970s, the development of nonreducible dielectrics was mainly achieved by the addition of acceptors such as MnO and Cr_2O_3.[18–20] As shown in eq. (4), it is considered that conduction electrons are trapped by the acceptors so that the decrease in insulating resistance is suppressed.

$$Mn_{Ti}'' + V_O^{\bullet\bullet} \rightarrow (Mn_{Ti}''V_O^{\bullet\bullet})^{*} \quad (4)$$

In the 1980s, Sakabe *et al*.[21] found that nonreducible $BaTiO_3$-based dielectrics were obtained by including a small amount of excess BaO in the BaO/TiO_2 ratio and by the addition of CaO. They reported that a small amount of CaO dissolved into the TiO_2 site under the condition of *A*-site excess, and CaO acted as an acceptor similar to MnO.[22,23] On

Table III. Dielectric ceramics materials for BME-MLCCs.

Designation	Base material	Additive
X7R(BX)	$(Ba_{1.02}Mg_{0.01})O_{1.003}(Ti_{0.99}Zr_{0.01})O_3$	La, Nd, Sm, Gd, Dy, Ho and Er oxides (0 to 2 at.%) Li_2O–SiO_2–CaO glass (0.5 wt%)
Y5V	$(Ba_{0.948}Ca_{0.05}Mg_{0.005})O_{1.003}(Ti_{0.86}Zr_{0.14})O_3$	La, Nd, Sm, Gd, Dy, Ho and Er oxides (0 to 2 at.%) Li_2O–SiO_2–CaO glass (0.5 wt%)

the other hand, Desu[24] reported that nonreducibility of $BaTiO_3$ was enhanced by the formation of Ba_2TiO_4 grain boundary phases instead of CaO working as an acceptor.

Dielectrics that are stable against firing atmospheres by *A*-site excess and addition of acceptors such as MnO have been developed and their practical applications have been intensively investigated.[25] However, $BaTiO_3$-based materials with excess *A*-site exhibit poor sinterability and the resulting chip components exhibit poor humidity resistance. Therefore, by adding a Li_2O–CaO–SiO_2 glass component having a high insulation resistance under a reducing atmosphere, we[26,27] developed low-temperature sinterable nonreducible $BaTiO_3$-based dielectrics that can be sintered at a relatively low temperature of about 1200°C and had *K* values comparable with that of conventional Pd electrode materials, and mass production of Y5V and X7R Ni-MLCC was started in the second half of the 1980s.

However, these materials based on the addition of acceptors exhibit an extremely short life property of insulation resistance at high temperatures and high electric fields compared with conventional MLCCs using Pd electrodes.[28] Hence, further thinning of the dielectric layers is difficult in view of reliability. Various models have been proposed to explain the mechanism of the degradation of the insulation resistance of the dielectrics. They may be classified into 1) grain boundary model[29,30] (High electric field across the grain boundaries generated by a Maxwell-Wagner polarization leads to a local dielectric breakdown process.), 2) reduction model[31–34] (The pile up of electromigrated oxygen vacancy at the cathode leads to reduction of the ceramics towards to the anode.), and 3) de-mixing model[35,36] (By electromigration of oxygen vacancies, the enrichment of oxygen vacancies near the cathode and depletion near the anode leads to the enhancement of the electronic charge carrier concentration between the electrodes resulting in the *pn* junction formation.) These models assume that the oxygen vacancies are an essential part of the degradation process. Thus, in the case of the acceptor-doped nonreducible dielectics, it is considered that a large insulation resistance degradation rate is due to the generation of the oxygen vacancies by the acceptor dopant as shown in eq. (4). On the other hand, it is well known that degradation of insulation resistance of dielectrics in a high electric field strongly depends on the donor-to-acceptor ratio of the added components.[37]

Fujikawa *et al*.[38] developed nonreducible $BaTiO_3$-based dielectrics containing Y_2O_3 and MnO in 1986. However, the role of Y_2O_3 was not clear. In the early 1990s, we had an interest in rare-earth elements having ionic radii between those of Ba and Ti ions and which can be dissolved in both the Ba and Ti sites, and investigated the effects of the addition of various rare-earth elements to nonreducible *A*-site excess $BaTiO_3$ dielectrics containing MgO and a Li_2O–CaO–SiO_2 glass component, as shown in Table III.[39–43] Table IV shows ionic radii of Ba, Ti, rare-earth elements, and Mg taken from Shannon's table.[44] In the table, ion radii of Dy, Ho, Y, Er, and Yb in 12 coordinates are obtained by extrapolation from the relationship between the coordination number and the ion radius. The ionic radius of a rare-earth element decreases by lanthanide contraction as the atomic number increases. Takada *et al*.[45] reported, based on the measurement of equivalent electrical conductivity at high temperatures that rare-earth elements dissolve in both the *A*- and *B*-sites depending on the *A*/*B* ratio in $BaTiO_3$. In addition, by computer simulation of energy of lattice defects, Lewis and Catlow[46,47] reported that rare-earth elements having intermediate ionic radii can dissolve in both the *A*- and *B*-sites. The rare-earth elements are believed to act as a donor when they dissolve in the Ba site or as an acceptor when they dissolve in the Ti site, as represented by

$$\text{Ba site: } R_2O_3 \rightarrow 2R_{Ba}^{\bullet} + V_{Ba}'' + 3O_O \quad (5)$$

Table IV. Effective ionic radii of various elements. (The ionic radii of Dy, Ho, Y, Er and Yb ion in 12 coordinate are based on the relationship between coordination number and effective ionic radius based on Shannon's table.[44])

Ion	Ionic radius (Å)	
	6 coordination	12 coordination
Ba^{2+}		1.610
Ti^{4+}	0.605	
Mg^{2+}	0.720	
La^{3+}	1.032	1.360
Sm^{3+}	0.958	1.240
Dy^{3+}	0.912	*1.255
Ho^{3+}	0.901	*1.234
Y^{3+}	0.900	*1.234
Er^{3+}	0.890	*1.234
Yb^{3+}	0.868	*1.217

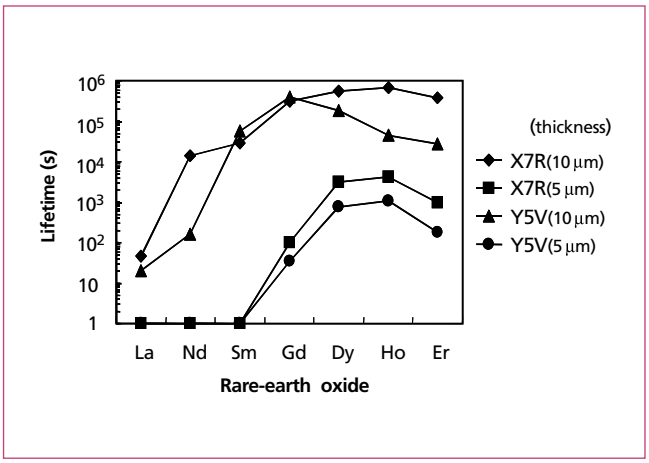

Fig. 5. Effect of the thickness of dielectric layers on the lifetime of Ni-MLCCs with 1at.% of various rare-earth ions.

Ti site: $R_2O_3 \rightarrow 2R_{Ti}' + 2O_O + V_O^{\bullet\bullet}$. (6)

We found that samples containing rare-earth elements exhibited significantly improved life characteristics when cooling below 1000°C in a firing process was carried out in a weakly oxidizing atmosphere not causing oxidation of nickel electrodes. Figure 5 shows a comparison of the results of a highly accelerated life test (HALT) at 350V and 165°C of X7R and Y5V Ni-MLCC samples with 1at.% rare-earth elements. Both the X7R and Y5V compositions exhibited excellent life characteristics by the addition of rare earth elements Dy_2O_3, Ho_2O_3, and Er_2O_3 having intermediate ionic radii even when the thickness of the dielectric layers was reduced to about 5μm. Furthermore, these Ni-MLCCs exhibit lifetimes comparable with or superior to that of conventional Pd-MLCCs. A combination of incorporation of rare-earth elements having specific ion radii and control of the cooling atmosphere in the firing enabled a significant improvement of life characteristics, and the development of thin-dielectric-layer Ni-MLCCs with large capacitance has been accelerated.

On the other hand, Nakano *et al.*[48] showed that the lifetime of Ni-MLCCs significantly improved by the addition of Y_2O_3 into nonreducible dielectrics. They studied the reason for the improved reliability and concluded that Y_2O_3 acts as a donor according to eq. (5) and compensates for oxygen vacancies caused by acceptors, such as MnO, which were added for enhancing nonreducibility. Since the ionic radius of Y_2O_3 is very close to that of Ho_2O_3 as shown in Table IV, their experimental results agreed well with our results. However, the reason why only rare-earth elements having specific ionic radii exhibited a significantly improved reliability are not yet sufficiently clarified and it is one of the subjects for future studies.

As described above, the reliability of the Ni-MLCCs strongly depends on the ionic radii of rare-earth elements. Therefore, it is considered that the reliability is related to the solubility states of rare-earth elements in $BaTiO_3$, such as the site occupancy and the amount of solid solution. The site occupancy of rare-earth element in the $BaTiO_3$ lattice could be strongly dependent on their ionic radius. Furthermore, a change in the ratio of dissolution in the *A*- and *B*-sites of rare-earth elements in $BaTiO_3$ should affect a change in the donor/acceptor ratio, which will have a strong effect on electrical characteristics.

In order to realize miniaturization and larger capacitance of the MLCCs, thinning of the dielectric layers is effective as shown in eq. (1). With a reduction in the thickness, the applied electric field significantly increases.

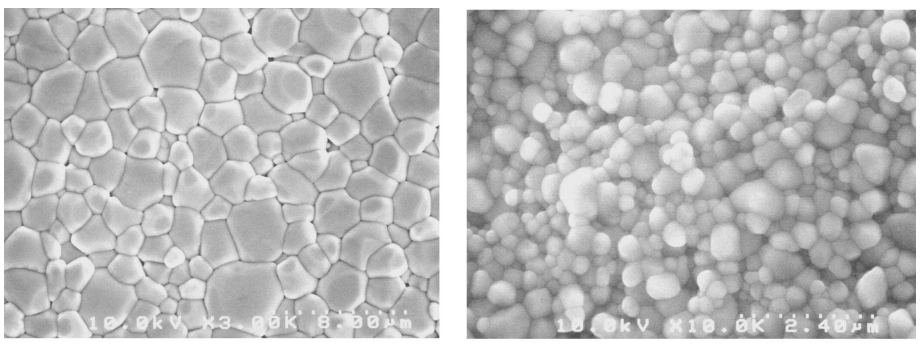

Fig. 6. SEM photographs of as-sintered surfaces. (a) Y5V, (b) X7R.

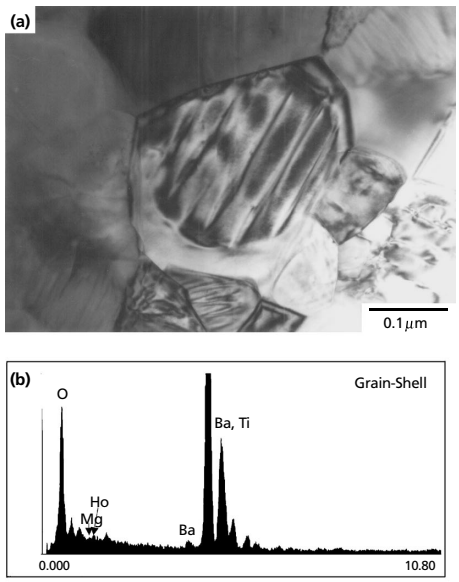

Fig. 7. (a) TEM photograph of grain and (b) EDX spectrum of grain shell of $BaTiO_3$–MgO–Ho_2O_3-based ceramics sintered at 1320°C.

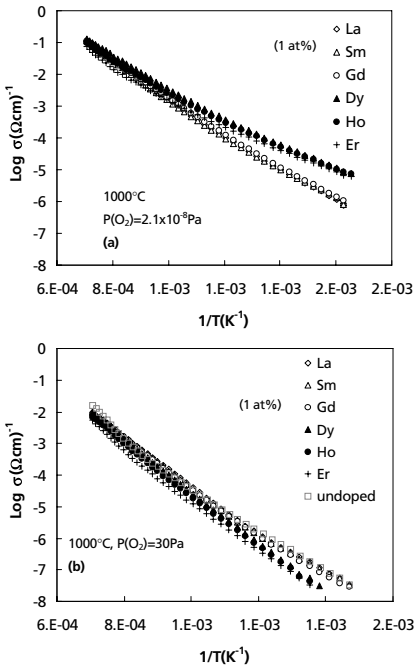

Fig. 8. Influence of Ho_2O_3 addition on the cooling stage in two different atmospheres. X7R composition: (a) reducing atmosphere, (b) weakly oxidizing atmosphere.

It is also well known that the degradation of insulation resistance of dielectrics at a high electric field strongly depends on the microstructures such as the grain size of the ceramics,[49] in addition to the composition such as the above-described donor/acceptor ratio. The control of microstructure has become more important to improve the reliability of MLCCs with a very thin dielectric layer less than 5μm. Figures 6(a) and 6(b) show scanning electron microscopy (SEM) photographs of surfaces of the Y5V and X7R samples. The Y5V sample shows uniform grain growth of about 3μm, whereas the X7R sample is composed of fine grains of below 0.5μm. In the X7R sample, the core-shell structure was formed as shown in the transmission electron microscopy (TEM) photograph [Fig. 7(a)]. An energy dispersive X-ray spectroscope (EDX) spectrum at a shell phase shown in Fig. 7(b) illustrates that MgO and Ho_2O_3 dissolve in $BaTiO_3$ in the shell. The core phase is composed of tetragonal ferroelectric almost pure $BaTiO_3$, and the shell phase is composed of a nonferroelectric solid solution of $BaTiO_3$ and additives.

In order to clarify the reason for a significant improvement in reliability of Ni-MLCCs by the addition of the rare-earth elements, we examined the effects of the addition of various rare-earth elements on dielectric properties and microstructures such as a core-shell structure, and also investigated the effect of the site occupancy of rare-earth elements in $BaTiO_3$ on the electrical properties and microstructure.

3. Effect of Rare-earth Doping

3.1 Dielectric properties and microstructure

The resistivity of $BaTiO_3$ ceramics at room temperature strongly depends on oxygen diffusion (re-oxidation) at the cooling stage during firing. Figure 8 shows changes in electrical conductivity of X7R samples, where one was sintered in a reducing atmosphere at 1200°C and then cooled at 350°C/h while maintaining the reducing atmosphere of $P(O_2)=10^{-8}$Pa, and the other was cooled after the firing atmosphere was changed to a weakly oxidizing atmosphere of $P(O_2)=30$Pa at 1000°C. The electrical conductivity strongly depended on the ionic radius of the rare-earth element. The intermediate ionic radius rare-earth (Dy_2O_3, Ho_2O_3, Er_2O_3)-doped samples showed higher electrical conductivity (lower resistivity) compared with the larger ionic radius rare-earth (La_2O_3, Sm_2O_3, Gd_2O_3)-doped samples, when they were cooled in a reducing atmosphere. However, in the case of the weakly oxidizing atmosphere, the Dy_2O_3-, Ho_2O_3-, and Er_2O_3-doped samples showed significantly lower conductivity (higher resistivity) than the La_2O_3-, Sm_2O_3-, and Gd_2O_3-doped samples. This result suggests that the rare-earth elements having intermediate ionic radii facilitate re-oxidation in the cooling stage and thus significantly decrease the number of oxygen vacancies in the samples compared with the larger ionic radius rare-earth elements. This result also agreed with the results on the HALT of Ni-MLCCs shown in the preceding section. Accordingly, it is considered that a significant improvement in lifetime is caused by a marked decrease in the oxygen vacancy concentration in the dielectrics due to the addition of the intermediate ionic radius rare-earth elements.

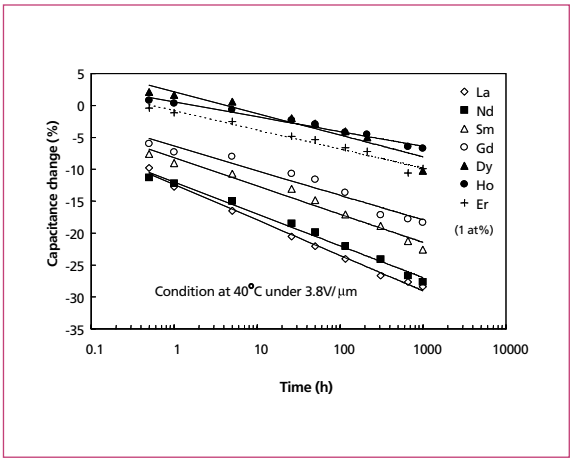

Fig. 9. Effect of rare-earth ions on capacitance change of X7R Ni-MLCCs during load life test.

It is desirable for the X7R MLCC that a change in capacitance be as small as possible before and after various reliability tests, in addition to flat temperature dependence. Figure 9 shows a change in capacitance of X7R Ni-MLCC samples containing various rare-earth elements after a load life test at 40°C and 50V for 1000h. Also in this case, the intermediate ionic radius rare-earth (Dy_2O_3, Ho_2O_3, Er_2O_3)-doped samples showed a smaller aging rate than those of the larger ionic radius rare-earth (La_2O_3, Sm_2O_3, Gd_2O_3)-doped samples. Hysteresis loops measured using the samples before and after the load life test showed that an increased change in capacitance over time was caused by an increased remanent polarization of the dielectrics. It is well known that a change in remanent polarization is caused by space charge in the dielectrics, such as an oxygen vacancy.[50–52] Figure 10 shows TEM photographs of samples containing Ho_2O_3 or Sm_2O_3. Both samples exhibited a core-shell structure. In the Sm_2O_3-doped sample, many dislocation loops were formed in the shell region with slight grain growth, whereas in the Ho_2O_3-doped sample, no substantial dislocation loop was observed. These dislocation loops were considered to be a set type of oxygen vacancies based on the analysis of the lattice image by high-resolution electron microscopy.[53,54] Thus, it is considered that the behavior on HALT and the change in capacitance during the load test strongly depends on the concentration of oxygen vacancies in the sample. Nomura *et al*.[55] analyzed the aging behavior of Ni-MLCCs during the load life test in detail and showed that the change followed a Richter-type relaxation curve having two relaxation times. They concluded that a change in capacitance in a short time period was caused by cation vacancies at grain boundaries and that in a long time period was caused by oxygen vacancies in the grains.

These results suggested that the solubil-

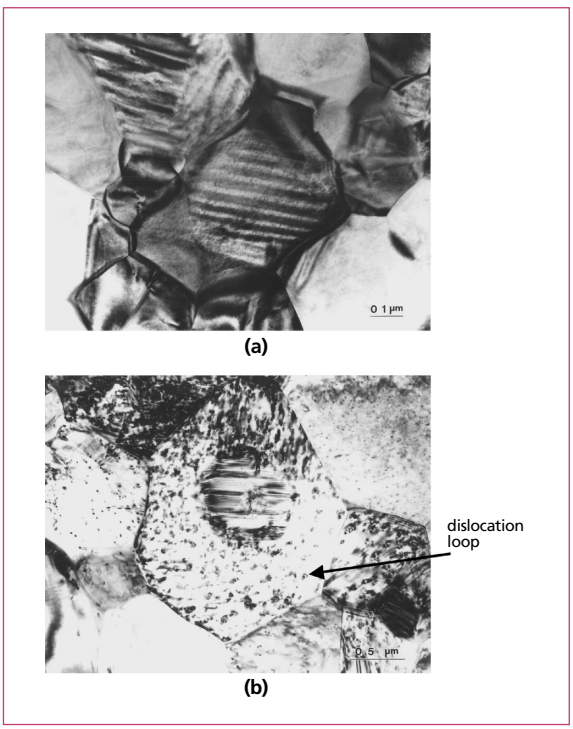

Fig. 10. TEM photographs of rare-earth-oxide-doped X7R ceramics. (a) Ho_2O_3, (b) Sm_2O_3.

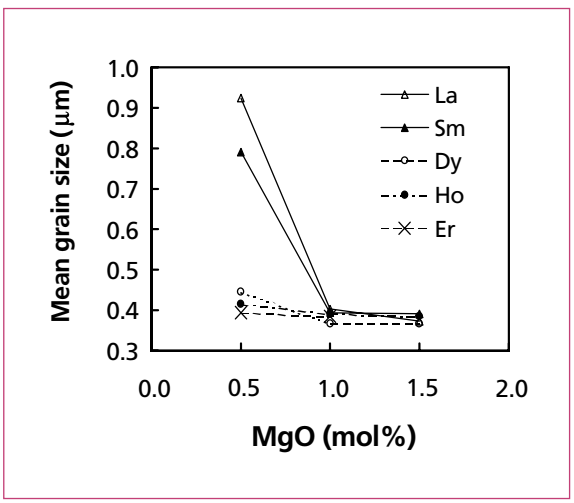

Fig. 11. Effect of MgO content on the mean grain size for the various rare-earth-oxide-doped samples.

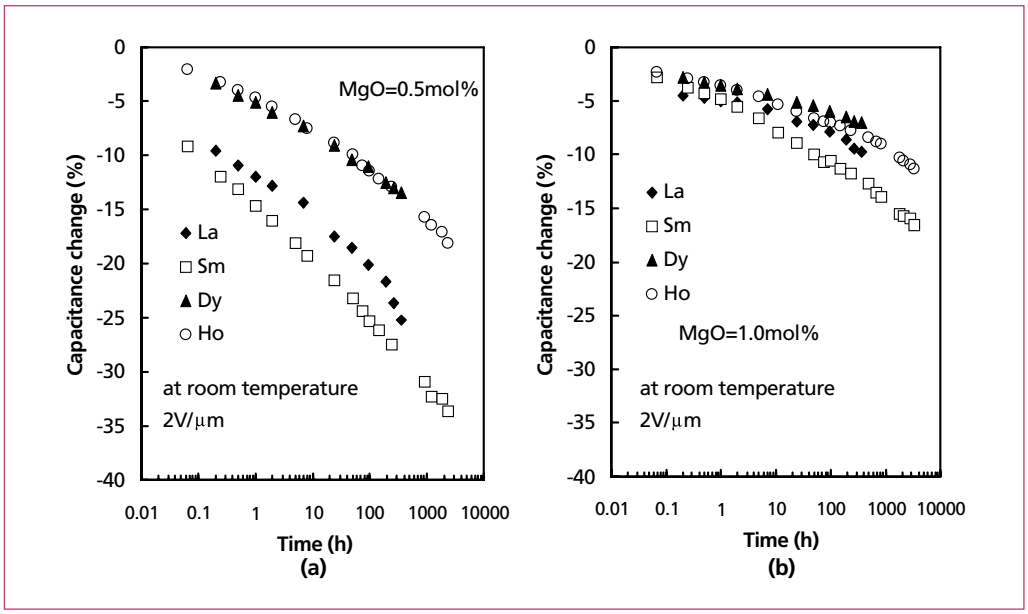

Fig. 12. Influence of rare-earth ions on the time-dependent change of capacitance under dc field for Ni-MLCCs. (a) MgO = 0.5 mol%, (b) MgO = 1.0 mol%.

ity states of rare-earth elements in the $BaTiO_3$ lattice depending on their ionic radii are closely related to the oxygen vacancy concentration in the samples and strongly affect the dielectric properties and reliability of Ni-MLCCs.

3.2 Core-shell formation behavior

Kishi *et al.*[56] investigated the influence of Mg and Ho_2O_3 on the formation behavior of the core-shell structure in the $BaTiO_3$–MgO–Ho_2O_3-based system, and reported the following: (1) MgO reacts with $BaTiO_3$ at low temperatures to form a shell phase; (2) Ho_2O_3 reacts with the shell phase at high temperatures; (3) MgO suppresses diffusion of Ho_2O_3 into the core and grain growth at high temperatures.

Furthermore, we examined the effects of various rare-earth elements on the formation of the core-shell structure in the $BaTiO_3$–MgO-rare-earth oxide (R_2O_3)-based system.[57,58] Figure 11 shows the effect of MgO content on the mean grain size for 1at.% various rare-earth-ion-doped samples. It was confirmed that a larger amount of MgO was necessary to suppress the grain growth and form the core-shell structure for the larger ionic radius rare-earth (La_2O_3, Sm_2O_3)-doped samples than for the intermediate ionic radius rare-earth (Dy_2O_3, Ho_2O_3, Er_2O_3)-doped samples. It seemed that the higher diffusivity into the core phase of La_2O_3 and Sm_2O_3 ions compared with Dy_2O_3, Ho_2O_3 and Er_2O_3 ions was related to their ionic radii.

The effect of the microstructure on the dielectric properties in the BT–MgO–R_2O_3-based system was also investigated.[59,60] It was found that a change in microstructure significantly affected the dielectric properties. Figure 12 shows the time dependence of the capacitance under a dc field of 2V/μm at room temperature. In all the samples, the aging rate decreased with increasing MgO content, but the change was relatively modest in the intermediate ionic radius rare-earth (Dy_2O_3, Ho_2O_3)-doped samples. In contrast, the larger ionic radius rare-earth (La_2O_3, Sm_2O_3)-doped samples showed a large dependence on the MgO content, and the sample containing 0.5 mol% MgO showed a significantly large aging rate due to the grain growth. However, the electrical properties of the La- and Sm_2O_3-doped samples were improved to a level near those of Dy_2O_3- and Ho_2O_3-doped samples when the MgO content was increased to form the core-shell structure.

To clarify the dependence of ionic radius of rare-earth ions on the microstructure of the BT–MgO–R_2O_3-based system, we investigated the effect of rare-earth element content and the firing temperature on the formation behavior of the core-shell structure using Dy_2O_3 and Ho_2O_3.[61,62] Figure 13 shows the mean grain sizes for the samples as a function of firing temperature. Although the ionic radii of Dy and Ho are very close, it appeared

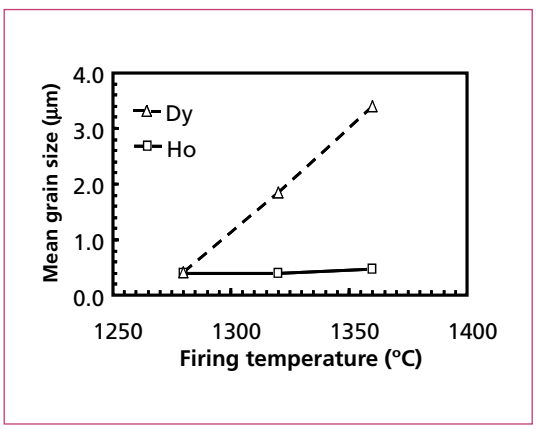

Fig. 13. Mean grain size of Dy_2O_3- and Ho_2O_3-doped disk samples as a function of firing temperature. (MgO = 0.5 mol%, R = 1.5 at.%).

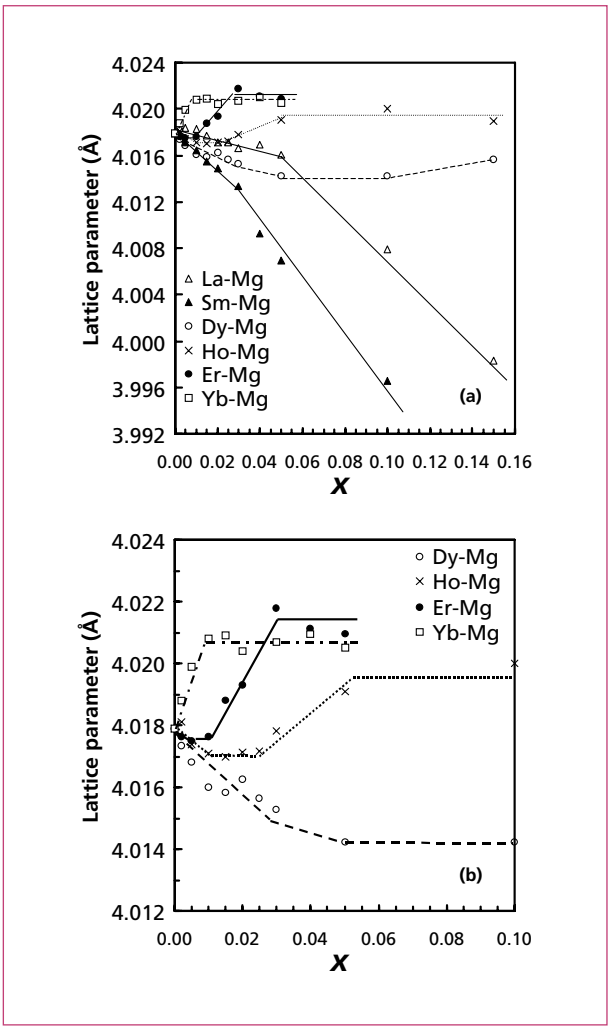

Fig. 14. Lattice parameters of $(Ba_{1-2x}R_{2x})(Ti_{1-x}Mg_x)O_3$ solid solutions measured at 300°C as a function of x (R = La, Sm, Dy, Ho, Er, Yb).

that their grain growth behaviors were clearly different. Dy_2O_3-doped samples showed grain growth as the firing temperature was increased, whereas Ho_2O_3-doped samples showed no grain growth. According to DSC and TEM observations, it was confirmed that the stability of Ho_2O_3-doped samples in the microstructure against firing temperature was much higher than that of Dy_2O_3-doped samples. The ionic radius of Dy is slightly larger than that of Ho. Hence, it is expected that there is a greater substitution of Dy into the *A*-site than into the *B*-site than that of Ho. This difference in the substitution of the rare-earth ions into the $BaTiO_3$ lattice should affect the microstructural evolution against firing temperature, such as the stability and the collapse of the core-shell structure. It was found that the control of the core-shell structure of the $BaTiO_3$–MgO–R_2O_3-based system required strict control of the MgO/R_2O_3 ratio and the firing condition, depending on the ionic radius of the rare-earth element.

3.3 Site occupancy study

As described above, the dielectric properties and microstructure of the $BaTiO_3$–MgO–R_2O_3-based system is strongly dependent on the ionic radius of the rare-earth element. Understanding the solubility state of rare-earth elements and MgO in the $BaTiO_3$ lattice is very important in improving the electrical properties of Ni-MLCCs. Therefore, to analyze the influence of rare-earth elements on the solubility in the shell phase of the $BaTiO_3$–MgO–R_2O_3-based system, we[63] synthesized the solid solutions by the conventional method according to following formula, assuming the shell phase of X7R dielectrics.

$$(Ba_{1-2x}R_{2x})(Ti_{1-x}Mg_x)O_3 \quad (7)$$

(x=0 to 0.15, R: rare earth element)

This formula is based on a model substituting rare-earth and Mg ions for Ba and Ti, respectively.

A single phase of $BaTiO_3$ solid solution was obtained in a wide range for the larger ionic radius rare-earth (La_2O_3, Sm_2O_3)-substituted samples compared with the Dy_2O_3-, Ho_2O_3-, Er_2O_3-, and Yb_2O_3-substituted samples. The lattice parameter of the samples was precisely measured by powder X-ray diffractometry (XRD) at 300°C, which was considerably higher than the Currie point, in order to avoid the influence of the phase transition due to the composition. Figure 14 shows the result of lattice parameters of the samples. In the case of the larger ionic radius rare-earth (La_2O_3, Sm_2O_3)-substituted samples, the lattice parameter decreased monotonously as a function of x. In the case of the intermediate ionic radius rare-earth (Dy_2O_3, Ho_2O_3, Er_2O_3)-substituted samples, both the decrease and the increase in the lattice parameters were observed. On the other hand, in the case of the smaller ionic radius rare-earth Yb_2O_3-substituted sample, the lattice parameter increased up to x=0.010 and showed no change above x=0.010. As a result, it was confirmed that larger ions (La,Sm) predominantly occupied the *A*-site, smaller ions (Yb) predominantly occupied the *B*-site and intermediate ions (Dy,Ho,Er) occupied both the *A*- and *B*-sites. It also appeared that the limit of solid solution of rare-earth ions in the $BaTiO_3$ lattice decreases as the ionic radius deceases. This phenomenon is closely related to the decrease in diffusivity of the rare earth element into the core phase as ionic radius decreases. Thus, it is considered that the stability of the core-shell structure against variation in the rare-earth content and firing temperature depends on the tendency for *B*-site occupation of the rare-earth element which is dependent on its ionic radius.

Figure 15 shows the electrical resistivity at room temperature of various rare-earth-substituted samples fired at 1380°C in a reducing atmosphere. In the case of the Dy_2O_3- and Ho_2O_3-substituted samples, a re-

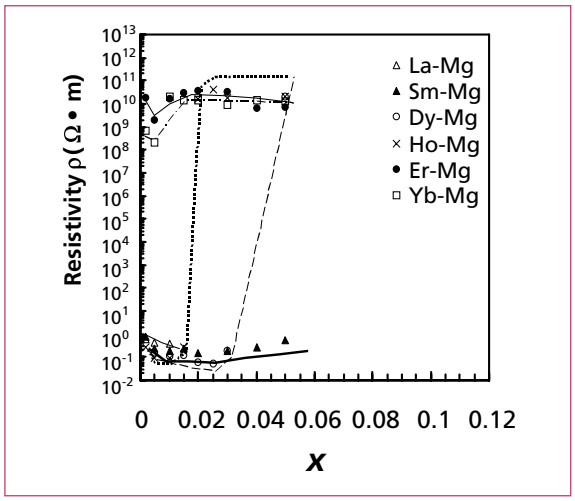

Fig. 15. Resistivities of $(Ba_{1-2x}R_{2x})(Ti_{1-x}Mg_x)O_3$ solid solutions sintered at 1380°C in a reducing atmosphere as a function of x (R = La, Sm, Dy, Ho, Er, Yb).

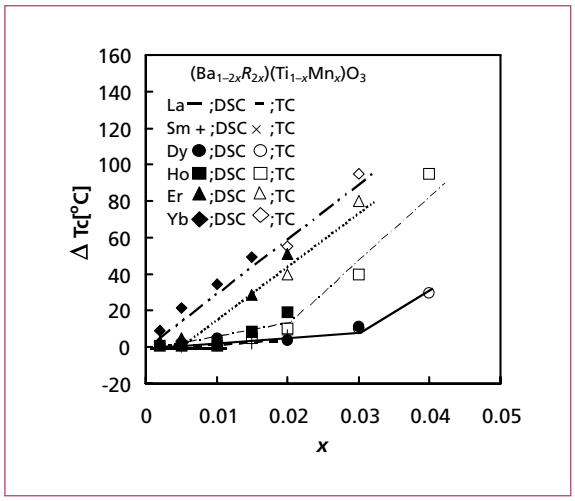

Fig. 16. Difference of T_c between the reduced and the re-oxidized state of $(Ba_{1-2x}R_{2x})(Ti_{1-x}Mn_x)O_3$ solid solutions as a function of x (R = La, Sm, Dy, Ho, Er, Yb, $\Delta T_c = T_c$(re-oxidized) – T_c(reduced)).

sistivity jump was observed. The change in resistivity substantially agreed with the change in lattice parameter. Thus, the resistivity jump of Dy_2O_3- and Ho_2O_3-substituted samples was attributed to the change of the predominant occupational site of Dy and Ho ions, from the *A*-site to the *B*-site. These results suggest that larger ions (La,Sm) predominantly act as donor dopants, smaller ions (Yb) as acceptor dopants, and intermediate ions (Dy,Ho,Er) as both donor and acceptor dopants.

Tsur *et al*.[64] also studied the site occupancy of rare-earth elements in $BaTiO_3$ with different *A*/*B* ratios by XRD measurements at room temperature, and found that the site occupancy of the rare earth element changed in response to the ionic radius and that Er_2O_3, Y_2O_3, Ho_2O_3, Dy_2O_3 and Gd_2O_3 occupied both the *A*- and *B*-sites, along with our results.

From these results, the significant improvement in reliability of Ni-MLCCs by the addition of intermediate rare-earth elements must be attributed to their amphoteric behavior as both a donor and an acceptor dopant in $BaTiO_3$ depending on the composition. These results also revealed that the occupancy ratio of rare-earth elements in the $BaTiO_3$ lattice strongly affected both the electrical properties and microstructure of Ni-MLCCs.

3.4 T_c shift by re-oxidation

As mentioned above, MnO is well known as an acceptor dopant for $BaTiO_3$, as well as MgO; the Mn ion acts as a divalent acceptor during firing in a reducing atmosphere, like the Mg ion. However, Mn^{2+} is easily oxidized to Mn^{3+} or Mn^{4+} by re-oxidation treatment, while Mg^{2+} maintains a constant valency. Albertsen *et al*.[65] reported the changes in the Curie point (T_c) under reduction and re-oxidation of $BaTiO_3$ ceramics containing MnO acceptors and various donor dopants on the *B*-site. With increasing donor concentration, the change in T_c after re-oxidation treatment is suppressed. They deduced that the formation of donor–acceptor complexes suppressed the valence change of Mn^{2+} to Mn^{3+} or Mn^{4+}. Thus, for the control of the electrical properties of the nonreducible dielectrics containing a rare-earth element and an acceptor dopant, the relationship between the site occupancy of the rare-earth element and the valence state of the acceptor must be clarified.

We prepared the MnO-containing shell phase model solid solution of $(Ba_{1-2x}R_{2x})(Ti_{1-x}Mn_x)O_3$ ($x \leq 0.100$), in addition to the MgO-containing samples as described in the former section, and examined the effect of re-oxidation treatment in air at 1200°C on the solubility state and dielectric properties of the samples.[66–68] For the MgO-containing samples, no change in the lattice parameter and T_c by re-oxidation was observed. In contrast, for the MnO-containing samples, changes in the lattice parameter and T_c were observed in a region in which the rare-earth element predominantly occupied the *B*-site. The intensity of electron spin resonance (ESR) spectra of Mn^{2+} in the MnO-containing samples was also strongly depressed in a region in which the rare-earth element predominantly occupied the *B*-site. Thus, it was considered that the changes in lattice parameter and T_c of the MnO-containing sample by reoxidation treatment were due to the valence change of Mn^{2+} to Mn^{3+} or Mn^{4+}. Figure 16 shows changes in T_c of MnO-containing samples by re-oxidation treatment. The larger ionic radius rare-earth (La_2O_3, Sm_2O_3)-substituted samples in which the rare-earth elements occupied the *A*-site exhibited no change in T_c, whereas the Dy_2O_3-, Ho_2O_3-, Er_2O_3-, and Yb_2O_3-substituted samples exhibited a shift of T_c toward high temperatures in a composition in which rare-earth elements predominantly occupied the *B*-site. Albertsen *et al*.[65] found that Mn^{2+} in donor–acceptor charge complexes could not be oxidized, and the T_c of reduced and re-oxidized material coincided for equivalent concentrations of the Mn acceptor and donor. Our results well agreed with their results, and can be explained as follows. In the composition in which the rare-earth element occupies the *A*-site, the *R* donor concentration and the Mn^{2+} acceptor concentration in the *B*-site are equal, and the formation of donor –acceptor complexes $(2R_{Ba}^{\bullet}Mn_{Ti}'')^{*}$ suppresses a change in the valence of Mn^{2+}; hence, a change in the lattice parameter and a shift

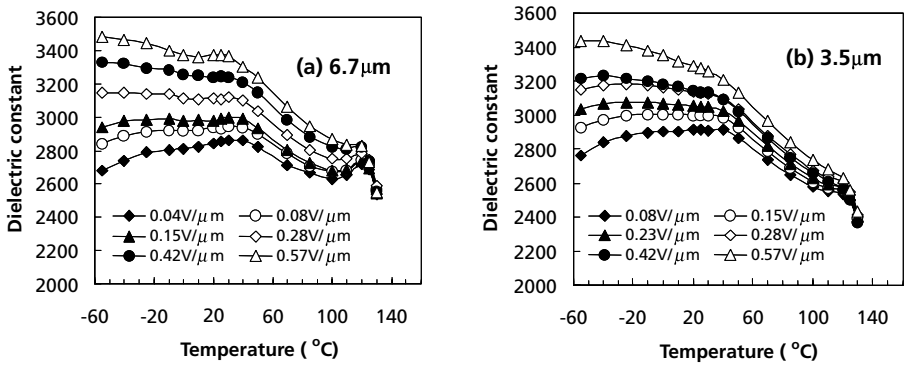

Fig. 17. Effect of AC electric field on temperature characteristics of dielectric constant for X7R Ni-MLCC with 6.7 μm and 3.5 μm layer thickness.

of T_c do not substantially occur during re-oxidation. In the composition in which the rare earth element predominantly occupies the *B*-site, increased *R* acceptors bring about an increase in the amount of free Mn^{2+} which can be re-oxidized into Mn^{3+} and Mn^{4+} during the re-oxidation, resulting in changes in the lattice parameter and T_c.

As a result, in nonreducible $BaTiO_3$-based dielectrics containing rare-earth elements and acceptor components, the site occupancy of the rare-earth elements strongly influenced not only the donor/acceptor ratio but also the valence of the acceptor component, and significantly affected the re-oxidation behavior and the resultant dielectric properties of Ni-MLCCs.

4. Electrical Properties of BME MLCCs

4.1 Effect of reduction of dielectric layer thickness

With trends toward thinner dielectric layer thickness and larger capacitance of Ni-MLCCs, the intensity of the electric field that is applied to the dielectric layers increases significantly. In particular, in the Y5V dielectrics involving grain growth, only one grain is present in a layer when the layer thickness decreases to about 3μm. Thus, it is important to understand a change in dielectric properties due to thinning of the layers and dielectric properties in a strong electric field. Chazono *et al*.[69] investigated the effect of AC electric field on Ni-MLCCs having various dielectric layer thicknesses using Y5V dielectrics based on $Ba(Ti,Zr)O_3$. As the thickness of the dielectric layer decreased, the peak of the *K* value broadened and shifted toward a lower temperature. Such a change in the temperature dependence of the *K* was approximately elucidated by the dependence of the intensity of the AC electric field applied to the dielectrics. Tsurumi *et al*.[70] proposed that the dependence of the AC electric field of $Ba(Ti,Zr)O_3$-based dielectrics could be explained by the existence of a polar micro region (PMR) on the basis of the model of the relaxors. We also examined the dependence of the dielectric layer thickness of X7R dielectrics. The *K* at a lower temperature of the X7R dielectrics at a constant measuring AC voltage of $1V_{rms}$, as well as that of the Y5V dielectrics, significantly changed as the thickness of the dielectric layer decreased. Figure 17 shows the dependence of the *K* of X7R MLCC samples having a dielectric layer thicknesses of 6.7μm and 3.5μm on the AC electric field. Also in the X7R dielectrics, the temperature dependence of the *K* at various thicknesses of the dielectric layer can be elucidated by the dependence of the intensity of the AC electric field, as in the Y5V dielectrics. Figure 18 shows the frequency dependence of the *K* of a X7R MLCC sample with a thickness of 3.5 μm. It was found that the shell phase showed a large frequency dependence since the dependence was observed below a temperature T_c of the core phase. Tsurumi *et al*.[71] also investigated the AC electric field dependence of the samples having a shell composition of X7R dielectrics and reported the shell phase was a relaxor because they showed an AC electric field dependence similar to that of $Ba(Ti,Zr)O_3$-based dielectrics.

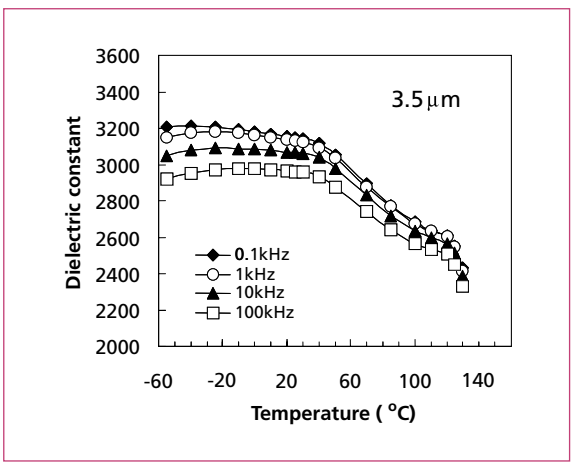

Fig. 18. Frequency dependence of dielectric constant for X7R Ni-MLCC.

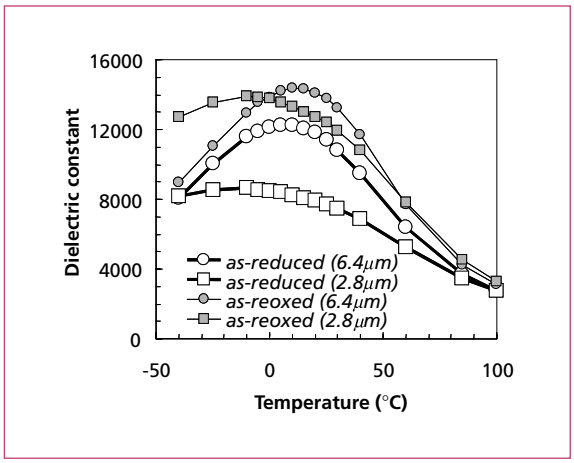

Fig. 19. Temperature dependence of dielectric constant for as-reduced and as-reoxidized sample having 2.8 μm and 6.4 μm layer thicknesses.

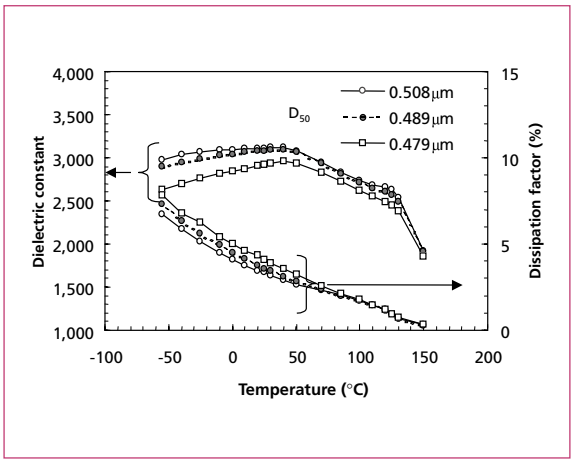

Fig. 20. Temperature dependence of the dielectric constant and dissipation factor for MLC samples fired at 1320°C.

On the other hand, Chazono *et al.*[72] reported re-oxidation of Y5V MLCCs having dielectric layer thicknesses of 2.8 μm and 6.4 μm. Figure 19 shows the temperature dependence of the *K* of the samples as fired in a reducing atmosphere and as re-oxidized in a weakly oxidizing atmosphere. By re-oxidation treatment, the *K* of the 2.8 μm sample increased by 60%, whereas that of the 6.4 μm sample increased by 15%. This difference suggested that oxygen vacancy generated during firing in a reducing atmosphere increased as the thickness of the dielectric layer decreased. A difference in the temperature dependence of the *K* value between the 2.8 μm sample and the 6.4 μm sample could be almost interpreted based on the AC electric field dependence, as described above. However, the temperature dependence of the *K* of the 2.8 μm sample was slightly broad and the *K* was low compared with those of the 6.4 μm sample. A possible reason for these phenomena is the effect of the amount of the oxygen vacancies generated during the firing. On the other hand, Nakano and Nomura[73] examined the effect of the layer thickness on the internal stress of MLCCs and reported that an increase in internal stress due to a reduction in layer thickness influenced the dielectric properties and lifetime. In order to achieve higher reliability of thin-layer Ni-MLCCs, further investigation on the relationships between the dielectric properties, the microstructure, the oxygen vacancies, and the internal stress is required.

4.2 Effect of microstructural evolution

Mizuno *et al.*[74] investigated the effect of the milling process for $BaTiO_3$–MgO–Ho_2O_3-based X7R dielectrics on the core-shell formation behavior and dielectric properties. The increase in the amount of milling medium resulted in the chipped particles of $BaTiO_3$ powders and the decrease of the $BaTiO_3$ crystallinity as shown in Table V. By careful TEM observation, grains were classified into the following three types: grains without a 90° domain pattern (named S-grain), grains showing only a 90° domain pattern (named C-grain) and grains showing a core-shell microstructure (named CS-grain). The rate of frequency for CS-grain increased, and that for C-grain decreased as the damage increased. The *K* value for MLCC samples with 3.5μm dielectric thickness decreased monotonously with the degree of damage increasing in all the measurement temperature ranges, as shown in Fig. 20. Furthermore, the peak of *K* at around room temperature shifted to a higher temperature as the degree of damage increased. These phenomena suggest that the decrease of *K* with increasing degree of damage was caused by the volumetric decrease of the core region composed of pure $BaTiO_3$. Figure 21 shows the results of HALT of MLCC samples. The leakage current decreased and the lifetime was prolonged as the degree of damage increased. It was suggested that the volumetric ratio of the shell region has an influence on the load lifetime characteristics of Ni-MLCC samples.

As described above, degradation of the insulation resistance of the dielectrics under simultaneous application of temperature and dc electric field is caused by electromigration of positively charged oxygen vacancies toward the cathode. Waser *et al.*[49] reported that grain boundaries acted as a barriers against the electromigration of oxygen vacancies. Furthermore, they analyzed the states of

Table V. Powder features and the rate of frequency for C-grain, CS-grains, and S-grains for samples.

	D_{50}(μm)	BET(m^2/g)	FWHM(°)	C-grain(%)	CS-grain(%)	S-grain(%)
Sample-1	0.508	3.53	0.1080	50	46	4
Sample-2	0.489	3.71	0.1113	48	45	7
Sample-3	0.479	4.40	0.1224	23	70	7

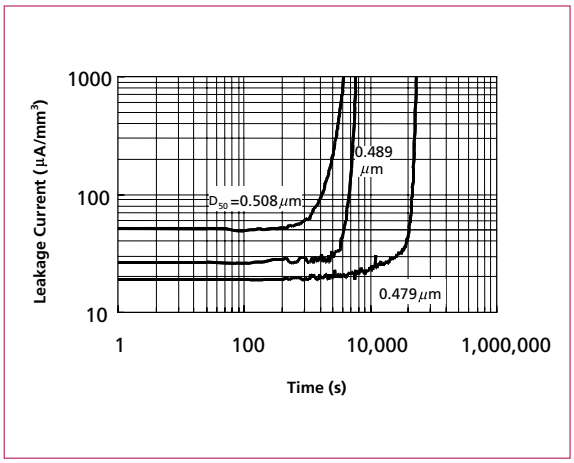

Fig. 21. Typical data of the time dependence of leakage current for MLC samples fired at 1320°C.

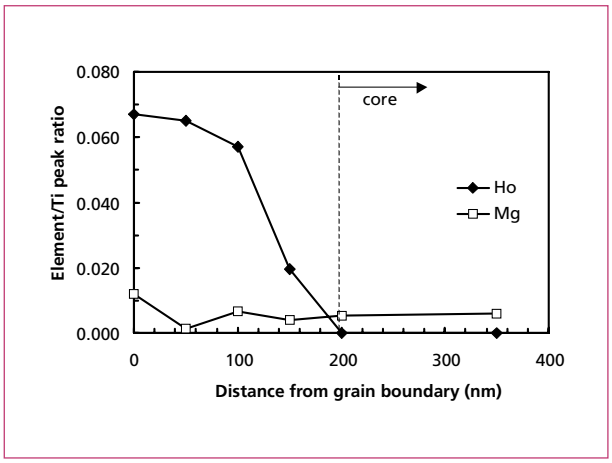

Fig. 22. Typical distribution of Ho_2O_3 and MgO in the grain for X7R samples as determined by TEM-EDX.

grain boundaries of acceptor-doped $SrTiO_3$ and $BaTiO_3$ by impedance spectroscopy, and proposed that a double Schottky barrier accompanied by a space charge depletion layer was formed at the grain boundaries. Chazono and Kishi[75] carried out impedance analysis of X7R Ni-MLCCs based on $BaTiO_3$–MgO –R_2O_3 dielectrics to clarify the relationship between the microstructure and the degradation of the insulation resistance. It was found that the electrical equivalent circuit corresponded to four sections, i.e., the core region, the shell region, the grain boundary, and the ceramic/Ni electrode interface region. Furthermore, they investigated the relationship between the result of impedance analysis and time dependence of the leakage current. At the initial stage, the leakage current was determined by the tunneling current passing through the grain boundaries, because the sample showed nonlinear *I–V* characteristics. As with time, the decrease in resistivity of the ceramic/electrode interface and the slight increase in resistivity of the core phase were observed. It was considered that the oxygen vacancies presented in the core phase migrated across the grain boundaries towards the cathode. At the final stage, the leakage current was determined by the decrease of resistance of the ceramic/electrode interface due to the pile up of oxygen vacancies near the cathode. Although, further investigation on the ceramic/electrode interface characteristic is still necessary, it is considered that the oxygen vacancy pile up brings about the decrease in resistance at the ceramic/electrode interface by either the physical change of the crystal lattice or change in the thickness of the ceramic/electrode interface. It appeared that the hindrance for the oxygen vacancy transport across the grain boundaries was not sufficiently large because of the small number of the grains between the internal electrodes in such a MLCC with a thin dielectric layer. This suggests that the insulation resistance degradation of X7R Ni-MLCCs is strongly affected not only by the state of the grain boundaries but also by the state of the ceramic/electrode interface.

Figure 22 shows the distribution of Ho_2O_3 and MgO in the grain for X7R dielectrics as determined by TEM and EDX. It was confirmed that Ho_2O_3 and MgO were distributed with gradient concentration from the grain boundary to the shell region. Kirianov *et al.*[76] also observed the distribution of Ho_2O_3 and MgO in the grain for X7R dielectrics with different Ho/Mg ratios, and reported that the behavior of gradient concentration of Ho_2O_3 and MgO in the shell phase is strongly dependent on the Ho_2O_3/MgO ratio. Further investigation of the compositional distribution, the concentration of the dopants, and the site occupancy of the rare-earth elements in the shell phase is necessary to elucidate the relationship between the change in microstructure and the electrical properties of X7R Ni-MLCCs.

5. Future Perspective

In recent decades, fabrication technology for thin-dielectric-layer Ni-MLCCs has made great progress and a dielectric thickness of 2μm has been achieved. Furthermore, technologies for further thinning are being developed. To realize high reliability of thin-dielectric-layer MLCCs, finer dielectric and electrode powders must be developed. Fine $BaTiO_3$ powder is being synthesized by wet processes, i.e., hydrothermal synthesis and a sol–gel process.[77] Hennings and Schreinemacher[78] reported that hydrothermally derived powder showed uniform grain distribution with satisfactory dispersion, but many micropores were present in a crystallite due to large amount of chemically bound OH groups. From TEM observation, sintered hydrothermal $BaTiO_3$ showed intergranular porosity. This porosity will adversely affect the dielectric properties of thinner dielectric layers. Thus, a new synthesis process for ultrafine particles having no defect is required. Also, fine Ni powder is being synthesized by the chemical vapor deposition (CVD) method or wet chemical process. Because the roughness of the electrode layer strongly affects the breakdown voltage of MLCC, control of agglomeration of fine Ni particles is an important subject.

Furthermore, handling of fine powders and thin sheets increases in difficulties as the layer thickness decreases, and current technologies are reaching their limits. Some new technologies are attempted for establishing

a ultrathin dielectric layer thickness of 1 μm or a submicron range. For the formation of thin layers, hydrothermal electrochemical synthesis, metallorganic chemical vapor deposition (MOCVD), and sol–gel synthesis are being tested. Takeshima *et al*.[79,80] succeeded in the development of a thin-layer MLCC of 15 dielectric layers with a thickness of 0.1 μm by MOCVD, using (Ba,Sr)TiO_3 as a dielectric and Pt as the electrode material. However, it is difficult to apply this to general MLCCs because of the high production cost; hence, this method is believed to be suitable for the formation of ultracompact capacitors on Si substrates. On the other hand, inexpensive layer forming processes, such as electrophoretic deposition (EPD) and inkjet printing, are being investigated.[81,82] It is important to establish monodispersion of fine particles into a solvent and to suppress cracking due to a large shrinkage during firing.

There are still growing demands for downsizing, high reliability and high-frequency performance of MLCCs. On the other hand, it is a disadvantage of $BaTiO_3$-based materials that Y5V and X7R Ni-MLCC showed large dependence of capacitance on an applied dc electric field. Improvement of dc bias characteristics and leakage current of dielectrics is strongly required for Ni-MLCCs with higher working voltage.

For replacing organic film capacitors to MLCCs, highly stable C0G characteristic Ni-MLCCs have also been developed and mass-produced using $CaZrO_3$-based dielectrics.[83,84] C0G Ni-MLCCs with large capacitance show stable electrical properties under high-voltage application because of their nonferroelectricity. It is expected that the amount of C0G Ni-MLCCs usage will increase in the near future.

In addition to requirements for larger capacitance of MLCCs, trends toward lower equivalent series resistance (ESR) and lower equivalent series inductance (ESL) are strengthened every year. Regarding lower ESR, development of Cu-electrode MLCCs using low-firing-temperature dielectric materials will be carried out intensively. Cu-MLCC for high-frequency application has already been mass-produced, using $CaZrO_3$-based dielectrics having a K value of about 30.[85] It is still necessary to study higher K materials having dense structure and good electrical properties even when fired at low temperatures below 1000°C. Regarding lower ESL, the current structure of MLCCs reaches the critical limit; hence, the formation of thin-film capacitors on a Si semiconductor or a circuit substrate is being investigated.[86]

There are still many problems for accomplishing highly integrated MLCCs with ultralarge capacitance of more than 100 μF. We must pay attention to both materials and process technologies to meet future requirements.

6. Conclusions

Recent progress in the field of non-reducible $BaTiO_3$-based dielectrics for MLCC with Ni internal electrodes was presented. Highly reliable Ni-MLCCs were obtained by the addition of intermediate ionic size rare-earth oxides such as Dy_2O_3, Ho_2O_3, Er_2O_3 and Y_2O_3. The effect of rare-earth dopants on the electrical properties and microstructure of the $BaTiO_3$–MgO–R_2O_3-based system was investigated. It was found that both the microstructure and electrical properties are strongly dependent on the change of site occupancy of rare-earth oxides in the $BaTiO_3$ lattice. It was also confirmed that the microstructure evolution had a close relationship to the electrical properties. Particularly, in EIA X7R specification dielectrics, distinctive electrical properties were obtained for the samples, which showed the collapse of the core-shell structure.

High-temperature powder XRD analysis and the resistivity results revealed that larger ions (La,Sm) occupy the A-site, intermediate ionic size (Dy,Ho,Er) ions occupy both the A- and B-sites, and smaller Yb ions occupy the B-site. It was determined that the site occupancy of intermediate ionic size rare-earths in $BaTiO_3$ lattice were effective for controlling the donor/acceptor dopant ratio and microstructure, and strongly affected the changes in T_c and dielectric properties for Ni-MLCCs by re-oxidation treatment.

The influence of the layer thickness for Ni-MLCCs was investigated. The temperature dependence of dielectric constant was greatly dependent on the layer thickness of less than 10 μm for both Y5V and X7R Ni-MLCCs. This behavior could be almost completely explained by the AC electric field strength. The dielectric properties of the shell phase in X7R dielectrics, as well as Y5V dielectrics, was explained as relaxor type.

As a parameter of the milling process, the effect of the microstructure evolution on the reliability of X7R Ni-MLCC was investigated. The leakage current decreased and the lifetime was prolonged as the degree of damage to $BaTiO_3$ powder increased. It was found that the reliability of Ni-MLCC is strongly dependent on the volumetric ratio of the core region to the shell region. The impedance of X7R Ni-MLCC was also investigated. All of the obtained data could be fitted to a 4-RC section electrical equivalent network. The electrical equivalent network was successfully correlated to the microstructure: the core, the shell, the grain boundary, and the ceramic/electrode interface. It was found that dc electrical degradation was well explained based on the electrical equivalent network.

Further investigations of the physical and chemical properties such as the compositional distribution, the concentration of the additives, and the site occupancy of the rare-earth oxides in nonreducible $BaTiO_3$-based dielectrics to realize highly reliable Ni-MLCCs with an ultrathin layer of less than 2 μm are required.

Acknowledgement

The authors are indebted to Professor T. Okuda and Professor H. Ohsato, Nagoya Institute of Technology, and Professor T. Tsurumi, Tokyo Institute of Technology, and Professor C. A. Randall, The Pennsylvania State University for their helpful advice and fruitful discussions. The authors would also like to thank Mr. Yamaoka and Mr. Fukui, Taiyo Yuden Co., Ltd., for their persistent encouragement, and Mr. Okino and Mr. Kohzu, Taiyo Yuden Co., Ltd. for their considerable cooperation.

JSAP

References

1) Y. Sakabe: *Proc. MRS Int. Meet. Advanced Materials*, Mater. Res. Soc. Symp. Proc. **10** (1989) 119.
2) Electrical Industry Alliance (EIA), World Capacitor Trade Statistics (WCTS) (2002).
3) K. R. Chowdary and E. C. Subbarao: Ferroelectrics **37** (1981) 689.
4) N. Yamaoka, M. Fukui and H. Nakamura: *Proc. 3rd Meet. Ferroelectric Materials and Their Applications*, Jpn. J. Appl. Phys. **20** (1981) Suppl. 20-4, p. 139.
5) I. Burn: J. Mater. Sci. **17** (1982) 1398.
6) D. Kumar, P. K. Sakharkar, O. Parkash and L. Pandey: J. Mater. Sci. Lett. **8** (1989) 652.
7) C.-H. Wang and L. Wu: Jpn. J. Appl. Phys. **32** (1993) 3518.
8) J. M. Haussone, G. Desgardin, P. Bajolet and B. Raveau: J. Am. Ceram. Soc. **66** (1983) 801.
9) I. Burn, M. T. Raad and K. Sasaki: Ceram. Trans. **8** (1990) 20.
10) G. A. Smolenskii, V. A. Isupov, A. I. Agranovskaya and S. N. Popov: Sov. Phys.-Solid State **2** (1961) 2584.
11) M. Yonezawa, K. Utsumi and T. Ohno: Proc. First Meet. Ferroelectric Materials and Their Applications, 1977, p. 297.
12) K. Furukawa, S. Fujiwara and T. Ogasawara: Proc. First US–Japan Study Semin. Dielectrics and Piezoelectric Ceramics, 1982, T-4.
13) J. Kato, Y. Yokotani, M. Nishida, S. Kawashima and H. Ouchi: *Proc. 6th Int. Ferroelectrocity*, Jpn. J. Appl. Phys. **24** (1985) Suppl. 24-2, p. 90.
14) T. R. Shrout and A. Halliyal: Am. Ceram. Soc. Bull. **66** (1987) 704.
15) Y. Yamashita, O. Furukawa, H. Kanai, M. Imai and M. Harata: Ceram. Trans. **8** (1990) 35.
16) K. Tsuzuku and M. Fujimoto: J. Am. Ceram. Soc. **76** (1994) 1451.
17) J. M. Herbert: Trans. Br. Ceram. Soc. **62** (1963) 645.
18) I. Burn and G. H. Maher: J. Mater. Sci. **10** (1975) 633.
19) N. G. Eror, I. Burn and G. H. Maher: U. S. Patent 3920781 (1975).
20) H. J. Hagemann and H. Ihrig: Phys. Rev. B **20** (1979) 3871.
21) Y. Sakabe, K. Minai and K. Wakino: *Proc. 3rd Meet. Ferroelectric Materials and Their Applications*, Jpn. J. Appl. Phys. **20** (1981) Suppl. 20-4, p. 147.
22) Y. H. Han, J. B. Appleby and D. M. Smyth: J. Am. Ceram. Soc. **70** (1987) 96.
23) D. Hennings and H. Schreinemacher: J. Eur. Ceram. Soc. **15** (1995) 795.
24) S. B. Desu: Key Eng. Mater. **66&67** (1992) 375.
25) Y. Sakabe: Am. Ceram. Bull. **66** (1987) 1338.
26) H. Kishi, T. Wada, S. Murai, H. Chazono and N. Yamaoka: Proc. Third US–Japan Semin. Dielectric and Piezoelectric Ceramics, 1986.
27) H. Kishi, S. Murai, H. Chazono, M. Ohshio and N. Yamaoka: *Proc. 6th Meet. Ferroelectric Materials and Their Applications*, Jpn. J. Appl. Phys. **26** (1987) Suppl. 26-2, p. 31.
28) S. Sumita, M. Ikeda, Y. Nakano, K. Nishiyama and T. Nomura: J. Am. Ceram. Soc. **74** (1991) 2739.
29) E. Loh: J. Appl. Phys. **53** (1982) 6229.
30) H. Neumann and G. Arlt: Ferroelectrics **69** (1986) 179.
31) K. Lehovec and G. A. Shirn: J. Appl. Phys. **33** (1962) 2036.
32) J. B. McChesney, P. K. Gallagher and F. V. DiMarcello: J. Am. Ceram. Soc. **46** (1963) 197.
33) K. Okazaki and H. Igarashi: Ferroelectrics **27** (1979) 263.
34) J. Rodel and G. Tomandl: J. Mater. Sci. **19** (1984) 179.
35) T. Baiatu, R. Waser and K.-H. Hardtl: J. Am. Ceram. Soc. **73** (1990) 1663.
36) J. Sheng, T. Fukami and J. Karasawa: J. Electrochem. Soc. **145** (1998) 1592.
37) R. Waser: J. Am. Ceram. Soc. **72** (1989) 2234.
38) N. Fujikawa, T. Shintome, H. Utaki and N. Yokoe: Proc. IMC 1986, 1986, p. 202.
39) H. Saito, H. Chazono, H. Kishi and N. Yamaoka: Jpn. J. Appl. Phys. **30** (1991) 2307.
40) H. Shizuno, S. Kusumi, H. Saito and H. Kishi: Jpn. J. Appl. Phys. **32** (1993) 4380.
41) H. Kishi and N. Yamaoka: *Science of Ceramic Interfaces II*, ed. J. Nowotny (Elseiver, Amsterdam, 1994) p. 613.
42) Y. Okino, H. Shizuno, S. Kusumi and H. Kishi: Jpn. J. Appl. Phys. **33** (1994) 5393.
43) H. Kishi, Y. Okino and N. Yamaoka: Proc. Seventh US–Japan Semin. Dielectric and Piezoelectric Ceramics, 1995, p. 255.
44) R. D. Shannon: Acta Crystallogr. A **32** (1976) 751.
45) K. Takada, E. Chang and D. M. Smyth: *Advances in Ceramics*, eds. J. B. Blum and W. R. Cannon: Am. Ceram. Soc. **19** (1985) 147.
46) G. V. Lewis and C. R. A. Catlow: Radiat. Effects **73** (1983) 307.
47) G. V. Lewis and C. R. A. Catlow: J. Phys. Chem. Solids **47** (1986) 89.
48) Y. Nakano, A. Sato, A. Hitomi and T. Nomura: Ceram. Trans. **32** (1993) 119.
49) R. Waser, T. Baiatu and K. H. Hardtl: J. Am. Ceram. Soc. **73** (1990) 1645.
50) K. Okazaki and K. Nagata: J. Am. Ceram. Soc. **56** (1973) 82.
51) F. Chu, H. T. Sun, L. Y. Zhaung and X. Yao: J. Am. Ceram. Soc. **75** (1992) 2939.
52) T. Fukami and J. Karasawa: J. Ceram. Soc. Jpn **101** (1993) 394 [in Japanese].
53) M. Fujimoto: Ceramics **25** (1990) 1044 [in Japanese].
54) T. Suzuki, M. Ueno, Y. Nishi and M. Fujimoto: J. Am. Ceram. Soc. **84** (2001) 200.
55) T. Nomura, N. Kawano, J. Yamamatsu, T. Arashi, Y. Nakano and A. Sato: Jpn. J. Appl. Phys. **34** (1995) 5389.
56) H. Kishi, Y. Okino, M. Honda, Y. Iguchi, M. Imaeda, Y. Takahashi, H. Ohsato and T. Okuda: Jpn. J. Appl. Phys. **36** (1997) 5954.
57) H. Kishi, H. Chazono, N. Kohzu, Y. Okino, M. Honda and Y. Mizuno: *Ceramics: Getting into the 2000's—Part E*, ed. P. Vincenzini (Techna, Italy, 1999) Advances in Science and Technology, Vol. 17, p. 53.
58) H. Kishi, N. Kohzu, J. Sugino, H. Ohsato, Y. Iguchi and T. Okuda: J. Eur. Ceram. Soc. **19** (1999) 1043.
59) Y. Okino, N. Kohzu, Y. Mizuno, M. Honda, H. Chazono and H. Kishi: Key Eng. Mater. **157–158** (1999) 9.
60) H. Chazono, Y. Okino, N. Kohzu and H. Kishi: Ceram. Trans. **97** (1999) 53.
61) H. Kishi, N. Kohzu, Y. Okino, Y. Takahashi, Y. Iguchi, H. Ohsato, K. Watanabe, J. Sugino and T. Okuda: Ceram. Trans. **100** (1999) 33.
62) Y. Mizuno, Y. Okino, N. Kohzu, H. Chazono and H. Kishi: Jpn. J. Appl. Phys. **37** (1998) 5227.
63) H. Kishi, N. Kohzu, J. Sugino, H. Ohsato, Y. Iguchi and T. Okuda: J. Eur. Ceram. Soc. **19** (1999) 1043.
64) Y. Tsur, A. Hitomi, I. Scrymgeour and C. A. Randall: Jpn. J. Appl. Phys. **40** (2001) 255.
65) K. Albertsen, D. Hennings and O. Steigelmann: J. Electroceram. **2** (1998) 193.
66) H. Kishi, N. Kohzu, Y. Iguchi, J. Sugino, M. Kato, H. Ohsato and T. Okuda: Jpn. J. Appl. Phys. **39** (2000) 5533.
67) H. Kishi, N. Kohzu, Y. Iguchi, J. Sugino, M. Kato, H. Ohsato and T. Okuda: J. Eur. Ceram. Soc. **21** (2001) 1643.
68) H. Kishi, N. Kohzu, N. Ozaki, H. Ohsato and T. Okuda: to be published in Proc. ISAF2002, IEEE.
69) H. Chazono, Y. Inomata, N. Kohzu and H. Kishi: Key Eng. Mater. **169–170** (1999) 31.

70) T. Tsurumi, Y. Yamamoto and N. Ohashi: Proc. Annu. Meet. Ceramic Society of Japan, 1999, p. 187 [in Japanese].
71) T. Tsurumi, H. Adachi, H. Kakemoto, S. Wada, Y. Mizuno, H. Chazono and H. Kishi: Jpn. J. Appl. Phys. **41** (2002) 6929.
72) H. Chazono, Y. Inomata, N. Kohzu and H. Kishi: Proc. Ninth US–Japan Semin. Dielectric and Piezoelectric Ceramics, 1999, p. 303.
73) Y. Nakano and T. Nomura: Proc. FMA-16, 1999, p. 7 [in Japanese].
74) Y. Mizuno, T. Hagiwara, H. Chazono and H. Kishi: J. Eur. Ceram. Soc. **21** (2001) 1649.
75) H. Chazono and H. Kishi: Jpn. J. Appl. Phys. **40** (2001) 5624.
76) A. Kirianov, T. Hagiwara, H. Kishi and H. Ohsato: Jpn. J. Appl. Phys. **41** (2002) 6934.
77) A. D. Hilton and R. Frost: Key Eng. Mater. **66–67** (1992) 145.
78) D. Hennings and H. Schreinemacher: J. Eur. Ceram. Soc. **9** (1992) 41.
79) Y. Takeshima, K. Shiratsuyu, H. Takagi and Y. Sakabe: Jpn. J. Appl. Phys. **36** (1997) 5870.
80) Y. Takeshima, K. Tanaka and Y. Sakabe: Ceram. Trans. **106** (2000) 441.
81) K. Yamashita, M. Matsuda, Y. Inda, T. Umegaki, M. Ito and T. Okura: J. Am. Ceram. Soc. **80** (1997) 1907.
82) J. Zhang and B. I. Lee: J. Am. Ceram. Soc. **83** (2000) 2417.
83) A. Sato, N. Oji, T. Kojima, S. Sato and T. Nomura: Key Eng. Mater. **157–158** (1999) 41.
84) T. Motoki, M. Naito, H. Sano, T. Konoike and K. Tomono: Jpn. J. Appl. Phys. **39** (2000) 5565.
85) Y. Yoneda, T. Kimura, T. Haratani and K. Asakura: Proc. CARTS Europe, 1997.
86) K. Kurihara and M. Ono: Denshi-Zairyo **41** (2002) 57 [in Japanese].

Hiroshi Kishi was born in Shizuoka Prefecture, Japan in 1955. He received his B.S. and M.S. degrees in Physics from Tokyo University of Science in 1978 and 1980, respectively. He joined Taiyo Yuden Co., Ltd., Materials Research and Development division in 1980. He obtained a Doctor's degree in Materials Science and Engineering from Nagoya Institute of Technology in 2002. His research interest is dielectric materials for multilayer ceramic capacitors and piezoelectric materials. He is an author and co-author of more than 50 scientific papers and 150 patents. He was rewarded the Richard M. Fulrath Awards from the American Ceramic Society in 1998. He is a member of the Ceramic Society of Japan and American Ceramic Society.

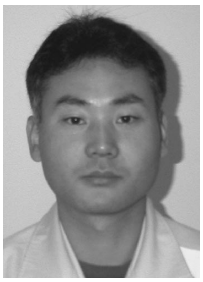

Youichi Mizuno was born in Aichi Prefecture, Japan in 1965. He received his B.S. degree in Inorganic Materials Engineering from Nagoya Institute of Technology in 1988. He joined Taiyo Yuden Co., Ltd., Materials Research and Development division in 1988. His research activities are nonreducible materials for Ni-MLCC and relaxor materials.

Hirokazu Chazono was born in Kagoshima Prefecture, Japan in 1959. He received his B.S. and M.S. degrees in Applied Chemistry from Keio University in 1983 and 1985, respectively. He joined Taiyo Yuden Co., Ltd. Materials Research and Development division in 1985. His research is focused on dielectric materials of multilayer ceramic capacitors and of electronic devices for high frequency usage. He is a member of the Ceramic Society of Japan and American Ceramic Society.